Inorganic Chemistry

Article

pubs.acs.org/IC

Polymorphism of Alkali Bis(fluorosulfonyl)amides (M[N(SO$_2$F)$_2$], M = Na, K, and Cs)

Kazuhiko Matsumoto,* Takaaki Oka, Toshiyuki Nohira, and Rika Hagiwara

Graduate School of Energy Science, Kyoto University, Yoshida, Sakyo-ku, Kyoto 606-8501, Japan

Supporting Information

ABSTRACT: The polymorphic behavior of Na, K, and Cs salts of the bis(fluorosulfonyl)amide anion N(SO$_2$F)$_2^-$ has been investigated by means of differential scanning calorimetry (DSC), single-crystal and powder X-ray diffraction, and Raman spectroscopy. All of the polymorphs observed in the present work (three for Na[N(SO$_2$F)$_2$], two for K[N(SO$_2$F)$_2$], and two for Cs[N(SO$_2$F)$_2$]) are stable enough for analyses at room temperature. With increasing temperature, form II of Na[N(SO$_2$F)$_2$] undergoes a solid−solid phase transition to form I, whereas another form (form III) crystallizes from the melt upon cooling. The anions in forms I and II of Na[N(SO$_2$F)$_2$] have trans and cis conformations, respectively, at 113 K, while cis−trans disorder is observed for the anion in form I at 298 K. Form I of K[N(SO$_2$F)$_2$], with a melting point of 375 K, is the stable form at room temperature, whereas solidification from the molten state during DSC gives rise to form II with a melting point of 336 K. Both forms I and II of K[N(SO$_2$F)$_2$] have anions in the cis conformation. The difference between the two potassium polymorphs arises from their crystal packing modes. In the case of Cs[N(SO$_2$F)$_2$], form I melts at 387 K, whereas form II undergoes a solid−solid transition to form I at 330 K. The anion of form I in Cs[N(SO$_2$F)$_2$] has an oxygen/fluorine disorder that exhibits an oxygen/fluorine eclipsed conformation, even at 113 K. The powder X-ray diffraction pattern of form II matches that of the previously known Cs[N(SO$_2$F)$_2$] structure of the trans conformer. Vibrational frequencies observed with Raman spectroscopy do not necessarily show the same trend as those calculated for the energy-minimized cis or trans conformers in the gas phase due to packing effects.

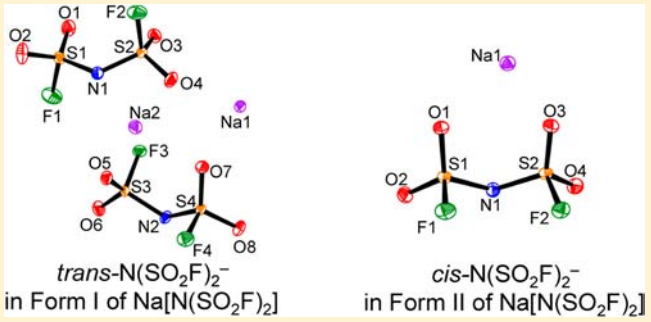

INTRODUCTION

The importance of fluorine-containing sulfonylamide anions for applications as electrolytes is now widely recognized.[1−5] Among these anions, N(SO$_2$F)$_2^-$ (often abbreviated as FSA or FSI) is highly significant owing to its excellent electrolyte properties. It is often used in the preparation of ionic liquid electrolytes because it gives salts with low melting point, high ionic conductivity, and low viscosity (e.g., 260 K, 16.5 mS cm^{-1}, and 24.5 cP, respectively for [EMIm][N(SO$_2$F)$_2$], where EMIm = 1-ethyl-3-methylimidazolium)[6] and high electrochemical stability.[2,6−9] Furthermore, the lithium derivative has attracted attention as an electrolyte in Li-ion batteries using organic solvents.[10−14]

The first example of a crystallographically investigated N(SO$_2$F)$_2$ group was FXeN(SO$_2$F)$_2$.[15,16] This compound was spectroscopically characterized before,[17,18] but this crystal structure confirmed the first Xe−N bond in the solid state. This was followed by the crystal structures of other examples, including the neutral acidic species HN(SO$_2$F)$_2$,[19] and salts of the N(SO$_2$F)$_2^-$ anion such as Li[N(SO$_2$F)$_2$],[20] K[N(SO$_2$F)$_2$],[19] and Cs[N(SO$_2$F)$_2$][21,22] and the Xe−N-bonded cation of [XeN(SO$_2$F)$_2$][Sb$_3$F$_{16}$].[23] According to recent computational studies,[24−26] gas-phase N(SO$_2$F)$_2^-$ has two energetic minima corresponding to approximate cis and trans conformers (with the trans conformer being more stable than the cis conformer), where cis and trans indicate the relative positions of the two F atoms, i.e., on the same side or opposite sides, respectively, relative to the plane defined by the S−N−S bonds. Although the molecular geometry in a crystal does not always correlate with that in the gas phase because of crystal-packing effects, the N(SO$_2$F)$_2^-$ anion conformation in crystals [and the N(SO$_2$F)$_2$ group in molecular compounds] has a geometry similar to that of the cis or trans conformer in many cases (e.g., a cis conformer is observed in Li[N(SO$_2$F)$_2$],[20] K[N(SO$_2$F)$_2$],[19] and [Ag(C$_6$H$_6$)][N(SO$_2$F)$_2$],[27] whereas a trans conformer is observed in FXeN(SO$_2$F)$_2$,[15,16] HN(SO$_2$F)$_2$,[19] Cs[N(SO$_2$F)$_2$],[21,22] [(C$_6$H$_5$)$_4$As][N(SO$_2$F)$_2$],[28] and [(CH$_3$)$_3$Pb][N(SO$_2$F)$_2$].[21] The small energy barrier between the two conformers affords free rotation about the S−N bonds to N(SO$_2$F)$_2^-$, and vibrational spectroscopy has shown that both conformers exist in the ionic liquid state.[24,25]

An interesting application of N(SO$_2$F)$_2^-$ salts is their use as inorganic ionic liquid electrolytes for secondary batteries.[29−32] In such an application, the melting point is an important factor and determines the operating temperature. The lowest melting point reported thus far for the N(SO$_2$F)$_2^-$ series of inorganic ionic

Received: May 20, 2012
Published: July 10, 2012

   dx.doi.org/10.1021/ic3010486 | Inorg. Chem. 2013, 52, 568−576

liquids is 309 K for $Na[N(SO_2F)_2]$:$K[N(SO_2F)_2]$:$Cs[N(SO_2F)_2]$ = 0.40:0.25:0.35, which is attractive for practical applications at temperatures above room temperature.[31]

Although the melting points of $M[N(SO_2F)_2]$ ($M = Li^+$, Na^+, K^+, Rb^+, and Cs^+) have been reported previously,[20,22,29−31] the irreproducibility of their thermal analyses has motivated us to study their possible polymorphism. Furthermore, if polymorphs exist for $M[N(SO_2F)_2]$, any correlation between known vibrational spectroscopic data[20,22] and crystal structures[19−22] should be reexamined. Considering that little research has been devoted to the polymorphism of $N(SO_2F)_2^-$ salts, we here report the identification of the polymorphs of $M[N(SO_2F)_2]$ (M = Na, K, and Cs) by detailed thermal analyses combined with single-crystal and powder X-ray diffraction (XRD) studies, as well as by Raman spectroscopy. Although this study focuses solely on alkali-metal salts, the understanding of polymorphism in the present systems will provide important insight into the thermal behavior of related compounds including their salts of organic cations.

RESULTS AND DISCUSSION

Thermal Behavior. Differential scanning calorimetry (DSC) curves of $M[N(SO_2F)_2]$ are shown in Figure 1. For $Na[N(SO_2F)_2]$, a small endothermic peak is observed at 375 K during the first heating process, followed by a large endothermic peak at 391 K. Powder XRD (Table S1 and Figure S1 in the Supporting Information, SI) reveals that the former peak is a solid−solid transition (from form II) and the latter is the melting point of form I. During the cooling process, supercooled $Na[N(SO_2F)_2]$ freezes at 326 K, forming another phase (form III) with a powder XRD pattern that is different from those of forms I and II (Figure S1 in the SI). In the second heating process, form III of $Na[N(SO_2F)_2]$ does not undergo a solid−solid phase transition and melts at 383 K, which is slightly lower than the melting point of form I.

The K salt, $K[N(SO_2F)_2]$, also shows two polymorphs designated as forms I and II, which have no relation to forms I and II of $Na[N(SO_2F)_2]$. As shown in the first scan, form I melts at 283 K, whereas form II appears at 326 K during the cooling process and melts at 336 K in the second heating process. The two phases exhibit different XRD patterns (Table S2 and Figure S2 in the SI). The powder XRD pattern of form I matches that of the previously known $K[N(SO_2F)_2]$ structure,[19] whereas form II has a novel structure (see the X-ray Crystal Structures section). Repetitive DSC analyses revealed that molten $K[N(SO_2F)_2]$ crystallized as form I only in some instances, which indicated that solidification into form I or II occurs under certain specific conditions (see the SI for details about the effects of vessels).

Powder XRD at room temperature of $Cs[N(SO_2F)_2]$ recrystallized from ethanol identified two different solid phases (forms I and II). Small differences in the experimental conditions (such as the levels of impurities and temperatures) seem to affect this behavior. Pure form I was sometimes obtained by recrystallization at 298 K, whereas pure form II could be reliably obtained by recrystallization at 253 K. In contrast to $Na[N(SO_2F)_2]$ and $K[N(SO_2F)_2]$, the solid−solid transition did not occur at room temperature for $Cs[N(SO_2F)_2]$. According to DSC, form I melts at 387 K, whereas form II shows a solid−solid phase transition to form I at 330 K, followed by melting at 387 K. According to powder XRD (Table S3 and Figure S3 in the SI), the crystal structure of form II agrees with the previously reported crystal structure,[21,22] whereas form I has a novel structure.

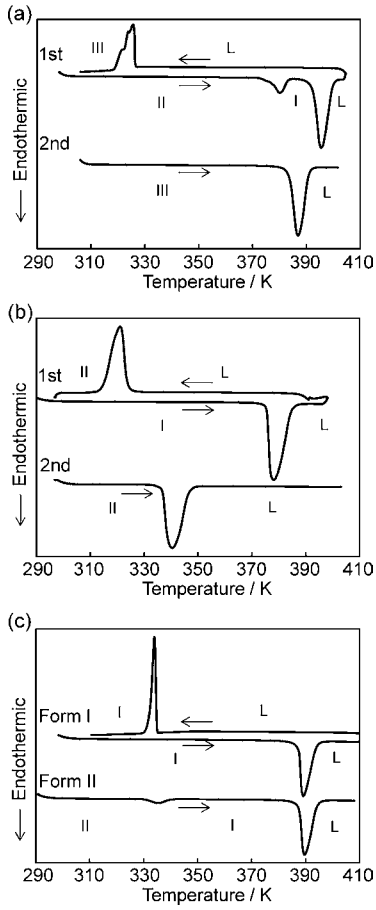

Figure 1. DSC thermograms for (a) $Na[N(SO_2F)_2]$, (b) $K[N(SO_2F)_2]$, and (c) $Cs[N(SO_2F)_2]$. Transition temperatures in K (enthalpy changes in kJ mol^{-1}) [phase transition]: 375 (3.5) [II → I], 391 (15.8) [I → L], 383 (15.3) [III → L], and 328 (10.0) [L → III] for $Na[N(SO_2F)_2]$, 375 (17.7) [I → L], 336 (16.0) [II → L], and 326 (14.9) [L → II] for $K[N(SO_2F)_2]$, and 330 (1.8) [II → I], 387 (17.6) [I → L], and 337 (12.7) [L → I] for $Cs[N(SO_2F)_2]$, where L is the liquid phase. Scan rate: 10 K min^{-1}.

X-ray Crystal Structures. Crystal data and refinement results for $Na[N(SO_2F)_2]$ (form I), $Na[N(SO_2F)_2]$ (form II), $K[N(SO_2F)_2]$ (form I), $K[N(SO_2F)_2]$ (form II), and $Cs[N(SO_2F)_2]$ (form I) at 113 K are given in Table 1 (see Table S4 in the SI for the values at 298 K). The relationship between the single-crystal structure and the phase in the DSC curves was confirmed by comparing the experimental powder XRD pattern with that of a powder pattern calculated from the single-crystal data (Figures S1−S3 in the SI). Important bond lengths and angles for the data at 113 K as well as those calculated for the gas-phase anion at the MP2/aug-cc-pVTZ level of theory (see Table S5 in the SI for the calculated geometrical parameters at the PBE1PBE/cc-pVTZ, PBE1PBE/aug-cc-pVTZ, and MP2/cc-pVTZ levels of theory) are listed in Table 2. Although the structure of $K[N(SO_2F)_2]$ (form I) at 150 K was reported in a previous work,[19] it was redetermined in this study in order to compare the data at 113 and 298 K with the other structures.

Figure 2 shows the ORTEP diagrams of the asymmetric units of the series of $N(SO_2F)_2^-$ salts at 113 K, as well as the optimized geometries of *cis*-$N(SO_2F)_2^-$ (C_1) and *trans*-$N(SO_2F)_2^-$ (C_2) at the MP2/aug-cc-pVTZ level of theory. The bond lengths and angles observed for $N(SO_2F)_2^-$ in the present structures are generally in good agreement with the previously reported

dx.doi.org/10.1021/ic3010486 | *Inorg. Chem.* 2013, 52, 568−576

Table 1. Summary of Crystallographic Data and Refinement Results for Polymorphs of $Na[N(SO_2F)_2]$, $K[N(SO_2F)_2]$, and $Cs[N(SO_2F)_2]$ at 113 K [or 143 K for $Cs[N(SO_2F)_2]$ (form II)[22]]

	$Na[N(SO_2F)_2]$ (form I)	$Na[N(SO_2F)_2]$ (form II)	$K[N(SO_2F)_2]$ (form I)	$K[N(SO_2F)_2]$ (form II)	$Cs[N(SO_2F)_2]$ (form I)	$Cs[N(SO_2F)_2]$ (form II)[a]
formula	$NaNS_2O_4F_2$	$NaNS_2O_4F_2$	$KNS_2O_4F_2$	$KNS_2O_4F_2$	$CsNS_2O_4F_2$	$CsNS_2O_4F_2$
fw	203.12	203.12	219.23	219.23	313.04	313.04
T/K	113	113	113	113	113	143
cryst system	monoclinic	monoclinic	orthorhombic	monoclinic	monoclinic	monoclinic
space group	$P2_1/n$	$P2_1/n$	$Pcab$	$P2_1/n$	$P2_1/n$	$P2_1/n$
a/Å	9.3056(9)	9.8209(5)	11.9661(3)	20.6477(9)	7.6219(5)	7.831(3)
b/Å	11.9158(8)	9.1050(4)	13.9120(4)	5.4979(4)	8.6364(7)	8.403(4)
c/Å	10.4106(8)	7.3238(4)	14.3913(5)	14.1674(9)	10.0207(8)	10.488(5)
β/deg	98.457(3)	119.814(3)	90	132.457(3)	91.225(2)	99.19(4)
V/Å^3	1141.81(16)	568.21(5)	2395.75(12)	1186.55(13)	659.47(9)	681.3
Z	8	4	16	8	4	4
ρ_{calc}/g cm^{-3}	2.363	2.374	2.431	2.454	3.153	–
μ/mm^{-1}	1.004	1.008	1.581	1.596	6.245	–
R_1[b]	0.0432	0.0275	0.0229	0.0679	0.0384	–
wR_2[c]	0.1115	0.0763	0.0623	0.1571	0.0952	–
cryst size/mm^3	0.50 × 0.50 × 0.80	0.10 × 0.10 × 0.10	0.20 × 0.20 × 0.30	0.30 × 0.50 × 0.50	0.30 × 0.50 × 0.60	–

[a] See ref 21. [b] $R_1 = \sum||F_o| - |F_c||/\sum|F_o|$. [c] $wR_2 = [\sum w(F_o^2 - F_c^2)^2/\sum w(F_o^2)^2]^{1/2}$.

values.[19−22,27,28] The F−S bond length is overestimated in all of the calculated structures, with the calculation at the MP2/aug-cc-pVTZ level of theory giving the best agreement [e.g., 1.546(2) and 1.560(2) Å for the trans conformer in $Na[N(SO_2F)_2]$ (form I) and 1.615 Å for the trans conformer calculated at the MP2/aug-cc-pVTZ level of theory]. The F1−S1−N1−S2 and F2−S2−N1−F1 torsion angles in the cis and trans conformers determined in the crystal structures also show some deviation from the calculated values. In particular, the F1−S1−N1−S2 angle of the trans conformer in $Na[N(SO_2F)_2]$ (form I) of 121.2(2)° is significantly larger than the calculated angle (75.4°). These differences suggest that the environment around the anion can change these torsion angles around the energetic minima.

Although both forms I and II of $Na[N(SO_2F)_2]$ belong to the monoclinic systems ($P2_1/n$), they have different $N(SO_2F)_2^-$ conformers (cis in form II and trans in form I at 113 K). As shown in their respective packing diagrams at 113 K (Figure 3), the conformational change from cis to trans (i.e., from form II) is accompanied by a change in the crystal packing. The alternating cation−anion layers in form II are distorted in form I, while the one-dimensional stacking mode of the anion also differs. The formula unit volume (V/Z) of form II (142.05 Å^3) is slightly smaller than that of form I (142.73 Å^3). An increase in the temperature causes positional disorder in form I, as shown in Figure 4. One of the two $N(SO_2F)_2^-$ anions in the asymmetric unit shows both trans and cis conformers with site occupancy factors of 0.705 and 0.295, respectively, at 298 K.[33] In this case, the F−S−N−S torsion angles are 90.2(4)° (F2A−S2−N1−S1) for the trans conformer and −70.0(5)° (F2B−S2−N1−S1) for the cis conformer. Form II, on the other hand, does not show disordering at 298 K.

Although both forms I and II of $K[N(SO_2F)_2]$ have *cis*-$N(SO_2F)_2^-$ geometries [F−S−N−S torsion angles = −69.07(11), 77.28(11), −73.79(11), and 71.08(12)° in form I and −76.0(6), 68.1(6), −74.0(6), and 72.4(6)° in form II], their packing modes and the resulting space groups are different (Figure 5). The structure of form I agrees with that described in the previous report,[19] and the unit cell belongs to the orthorhombic system (space group $Pcab$). Form II, which belongs to the monoclinic system (space group $P2_1/n$), has a distinct layered structure, with the anions forming a double layer in which the O atoms protrude from both sides and the cations are sandwiched between the anionic layers. Such a layered structure is not observed in form I. Disorder was not observed at 298 K in either form I or form II.

Form I of $Cs[N(SO_2F)_2]$ belongs to the monoclinic system (space group $P2_1/n$). Although this space group is the same as that of the previously reported $Cs[N(SO_2F)_2]$ structure with a trans conformer (form II in this work),[21,22] they have different crystal structures. The anion in form I has a structure based on the cis conformer but shows oxygen/fluorine disorder even at 113 K; i.e., two S−O/F bond lengths were shorter than the expected S−F bond and longer than the expected S−O bond. This type of disorder is frequently observed for oxofluoroanions and is therefore not unexpected for a $N(SO_2F)_2$ group (e.g., the same phenomenon is observed in the anions of $[(C_6H_5)_4As][N(SO_2F)_2]$,[28] $[(CH_3)_3Sn(dmi)_2][N(SO_2F)_2]$ (dmi = *N*,*N*′-dimethylethyleneurea),[21] and $[Ag(C_6H_6)][N(SO_2F)_2]$[27] as well as the cation of $[XeN(SO_2F)_2)][Sb_3F_{16}]$[23]). A detailed structural analysis of this disordering was reported for the structurally related SO_2F^- anion, which often showed oxygen/fluorine disorder where the observed S−O and S−F bond lengths were also found to be longer (for S−O) and shorter (for S−F) than estimated.[34] In the present $Cs[N(SO_2F)_2]$ (form I) salt, the disorder was observed even at 113 K. The oxygen/fluorine ratio at the O3A/F2B (F2A/O3B) site in Figure 2e is 0.72:0.28 at 113 K and is 0.37:0.63 at 298 K, which suggests that the cis conformer is dominant at lower temperatures, while the ratio of the eclipsed oxygen/fluorine conformation increases at higher temperature. The previously reported structure of $Cs[N(SO_2F)_2]$[21,22] is assigned to form II in this work based on the powder XRD results (Table S3 and Figure S3 in the SI). In contrast to the cis conformer in form I, the anion adopts a trans conformer in form II. The packing modes of the two Cs forms are compared in Figure 6. In both structures, the cation and anion layers stack along the *a* axis, but they do not perfectly overlap with each other (Figure 6a,b). The ion configurations within the layers in forms I and II are similar, and they are best described as a distorted NaCl-type structure (Figure 6c,d). The difference in the anion

dx.doi.org/10.1021/ic3010486 | *Inorg. Chem.* 2013, 52, 568−576

Table 2. Experimental Bond Lengths and Bond Angles for $N(SO_2F)_2^-$ in Polymorphs of $Na[N(SO_2F)_2]$, $K[N(SO_2F)_2]$, and $Cs[N(SO_2F)_2]$ at 113 K and Calculated Bond Lengths and Bond Angles for $N(SO_2F)_2^-$

	exp					calc MP2/aug-cc-pVTZ	
	$Na[N(SO_2F)_2]$ (form I), trans−trans	$Na[N(SO_2F)_2]$ (form II), cis	$K[N(SO_2F)_2]$ (form I), cis−cis	$K[N(SO_2F)_2]$ (form II), cis−cis	$Cs[N(SO_2F)_2]$ (form I), cis[a]	cis(C_1)	trans(C_2)
			Bond Lengths/Å				
S1−O1	1.413(3)	1.4331(11)	1.4252(13)	1.434(7)	1.422(4)	1.444	1.446
S1−O2	1.414(3)	1.4189(11)	1.4193(13)	1.410(6)	1.422(4)	1.443	1.443
S2−O3	1.415(3)	1.4222(11)	1.4216(13)	1.418(6)	1.450(4) (O3A)[a]	1.445	
S2−O4	1.430(2)	1.4234(11)	1.4247(12)	1.423(6)	1.420(3)	1.443	
S1−F1	1.546(2)	1.5564(10)	1.5649(11)	1.571(5)	1.568(3)	1.620	1.615
S2−F2	1.560(2)	1.5539(9)	1.5557(10)	1.558(5)	1.528(3) (F2A)[a]	1.621	
S1−N1	1.567(3)	1.5701(13)	1.5656(14)	1.558(7)	1.554(4)	1.590	1.590
S2−N1	1.554(3)	1.5739(13)	1.5732(14)	1.580(7)	1.570(4)	1.588	
S3−O5	1.435(2)		1.4276(13)	1.426(6)			
S3−O6	1.416(2)		1.4140(13)	1.424(6)			
S4−O7	1.432(2)		1.4178(12)	1.427(6)			
S4−O8	1.419(2)		1.4331(12)	1.411(6)			
S3−F3	1.553(2)		1.5776(11)	1.554(5)			
S4−F4	1.548(2)		1.5627(11)	1.577(5)			
S3−N2	1.574(3)		1.5802(14)	1.570(7)			
S4−N2	1.575(3)		1.5680(15)	1.561(7)			
			Bond Angles/deg				
S1−N1−S2	124.51(19)	123.90(9)	123.79(9)	123.9(5)	123.1(2)	121.4	119.7
N1−S1−F1	99.95(16)	103.78(6)	103.53(7)	102.5(3)	103.7(2)	102.8	102.8
N1−S2−F2	103.22(16)	102.97(6)	102.49(7)	104.3(3)	106.6(2) (F2A)[a]	101.2	
N1−S1−O1	115.93(16)	115.48(7)	116.16(8)	115.9(4)	116.9(2)	116.7	116.3
N1−S1−O2	109.94(17)	108.33(7)	108.73(8)	109.7(4)	108.4(2)	108.1	108.4
N1−S2−O3	118.38(16)	116.72(7)	117.00(8)	116.8(4)	112.4(2) (O3A)[a]	117.3	
N1−S2−O4	106.81(16)	106.38(7)	106.69(8)	106.2(4)	109.0(2)	108.8	
O1−S1−O2	118.64(18)	118.41(7)	117.62(8)	117.2(4)	117.4(2)	119.2	119.6
O3−S2−O4	118.40(16)	119.09(7)	119.06(8)	117.9(4)	114.6(2) (O3A)[a]	119.9	
O1−S1−F1	105.33(17)	103.66(6)	104.37(7)	104.8(4)	103.4(2)	103.6	103.7
O2−S1−F1	104.40(17)	105.51(6)	104.65(7)	104.9(3)	105.2(2)	104.2	103.6
O3−S2−F2	103.84(14)	104.71(6)	104.33(7)	104.8(3)	105.5(2) (O3A/F2A)[a]	103.2	
O4−S2−F2	104.01(15)	105.11(6)	105.27(7)	105.3(3)	108.3(2) (F2A)[a]	103.4	
S3−N2−S4	120.54(18)		123.68(9)	124.4(5)			
N2−S3−F3	103.39(14)		102.05(7)	104.2(3)			
N2−S4−F4	103.64(14)		104.01(7)	103.3(3)			
N2−S3−O5	114.77(15)		115.95(7)	116.9(4)			
N2−S3−O6	103.78(13)		108.46(8)	106.3(4)			
N2−S4−O7	115.99(15)		116.93(8)	115.7(4)			
N2−S4−O8	107.54(15)		107.11(7)	109.6(4)			
O5−S3−O6	118.59(15)		119.69(8)	117.8(4)			
O7−S4−O8	118.67(15)		118.23(8)	117.6(4)			
O5−S3−F3	103.78(13)		103.11(7)	104.5(3)			
O6−S3−F3	105.53(14)		105.23(7)	105.6(3)			
O7−S4−F4	103.93(14)		104.77(7)	104.0(3)			
O8−S4−F4	105.35(14)		103.98(7)	104.8(3)			
			Torsion Angles/deg				
F1−S1−N1−S2	121.2(2)	−72.31(11)	−69.07(11)	−76.0(6)	−69.5(3)	−62.5	75.4
F2−S2−N1−S1	79.4(3)	77.54(11)	77.28(11)	68.1(6)	68.0(3) (F2A)[a] −47.1(4) (F2B)[a]	88.5	
F3−S3−N2−S4	78.5(2)		−73.79(11)	−74.0(6)			
F4−S4−N2−S3	86.5(2)		71.08(12)	72.4(6)			

[a]Oxygen/fluorine disorder was observed. The S−F and S−O bond lengths were separately restrained by the DFIX instruction (see the Experimental Section for details).

conformation results in a slight difference in the cell parameters of forms I and II.

The coordination environments around the alkali metals in the present series of $N(SO_2F)_2^-$ salts are shown in Figure S4 in the SI; it is seen that the coordination numbers increase with increasing size of the cation. One of the two crystallographically independent Na^+ cations in $Na[N(SO_2F)_2]$ (form I) has an approximate octahedral coordination environment [Na−O bond

dx.doi.org/10.1021/ic3010486 | Inorg. Chem. 2013, 52, 568−576

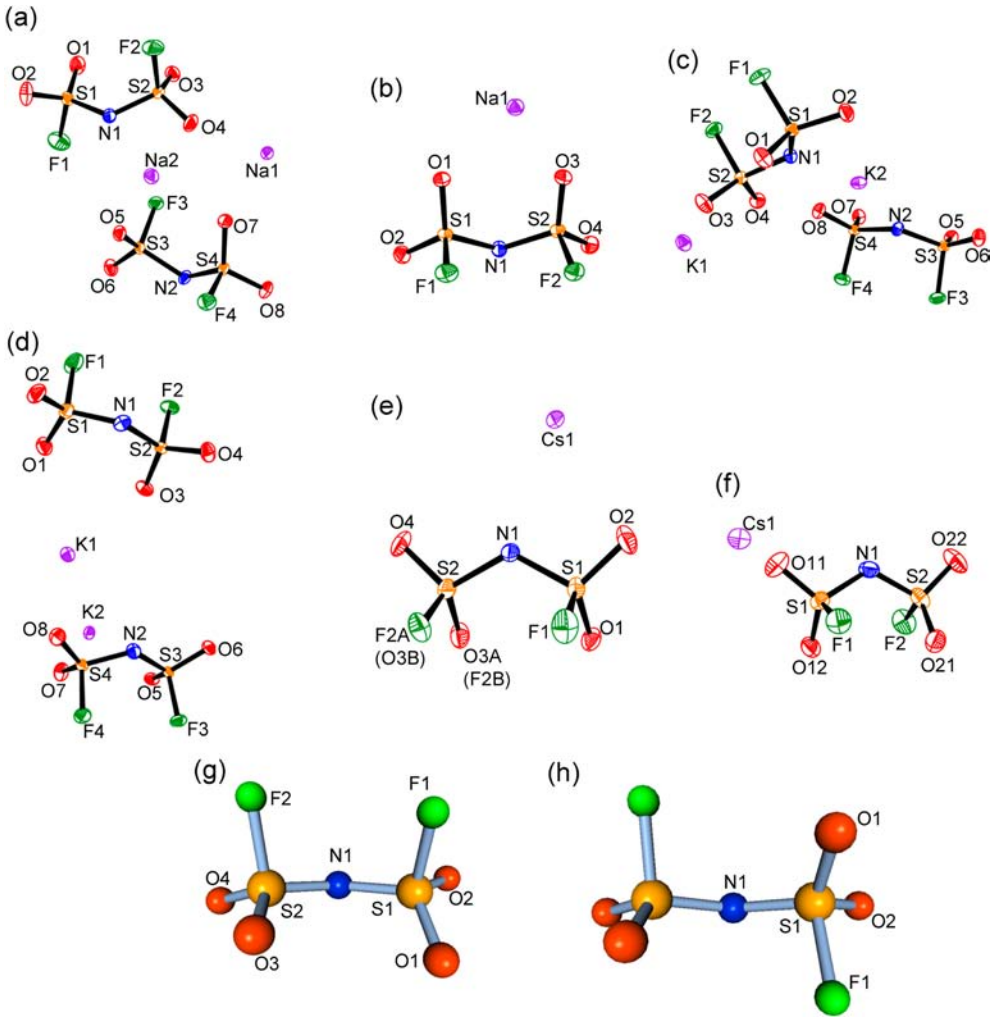

Figure 2. Asymmetric units of (a) $Na[N(SO_2F)_2]$ (form I), (b) $Na[N(SO_2F)_2]$ (form II), (c) $K[N(SO_2F)_2]$ (form I), (d) $K[N(SO_2F)_2]$ (form II), (e) $Cs[N(SO_2F)_2]$ (form I), and (f) $Cs[N(SO_2F)_2]$ (form II)[21] and optimized geometries of (g) *cis*-$N(SO_2F)_2^-$ and (h) *trans*-$N(SO_2F)_2^-$ at MP2/aug-cc-pVTZ. The thermal ellipsoids of the experimental structures are shown at the 50% probability level. The cis and trans designations refer to the positions of the two F atoms relative to the plane defined by the S−N−S bonds, i.e., on the same side (cis) or on opposite sides (trans).

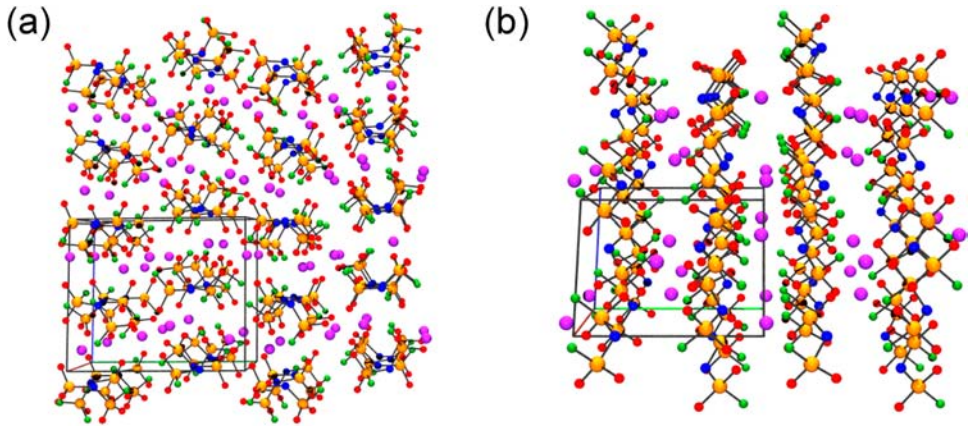

Figure 3. Packing diagrams of (a) $Na[N(SO_2F)_2]$ (form I) and (b) $Na[N(SO_2F)_2]$ (form II) along the *a* axis.

lengths = 2.308(3)−2.419(3) Å], whereas the other Na^+ has a distorted monocapped octahedral coordination environment [Na−O(−N) bond lengths = 2.354(3)−2.842(3) Å; O8 caps the octahedron]. The other form, $Na[N(SO_2F)_2]$ (form II), contains a single crystallographically independent cation that has an approximate monocapped octahedral coordination with Na−O bond lengths of 2.2885(12)−2.5610(13) Å and Na−N of 2.6204(15) Å, where O4 caps the octahedron. In all cases, the F atom is not involved in primary contacts with Na^+. The two K cations in $K[N(SO_2F)_2]$ (form I) are nine-coordinate: K1 is in a tricapped trigonal-prismatic environment [K−O bond lengths = 2.6590(13)−2.9705(13) and K−F bond length = 3.4079(12) Å;

dx.doi.org/10.1021/ic3010486 | *Inorg. Chem.* 2013, 52, 568−576

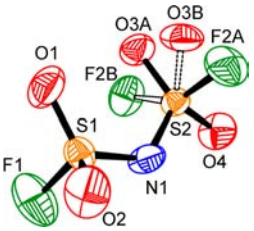

Figure 4. Disordered $N(SO_2F)_2^-$ in $Na[N(SO_2F)_2]$ (form I) at 298 K. Thermal ellipsoids are shown at the 50% probability level.

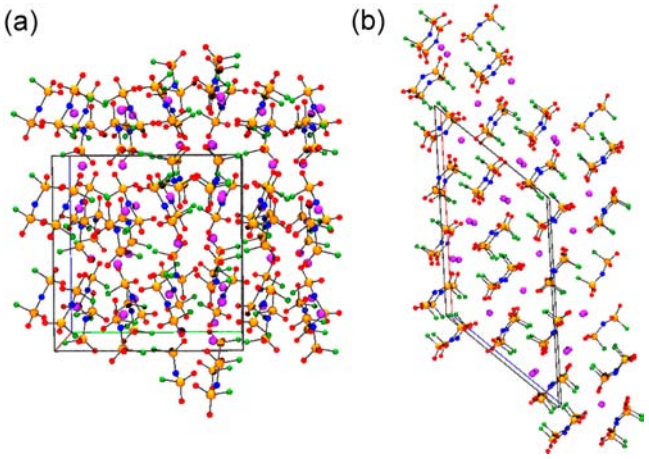

Figure 5. Packing diagrams of (a) $K[N(SO_2F)_2]$ (form I) viewed along the *a* axis and (b) $K[N(SO_2F)_2]$ (form II) viewed along the *b* axis.

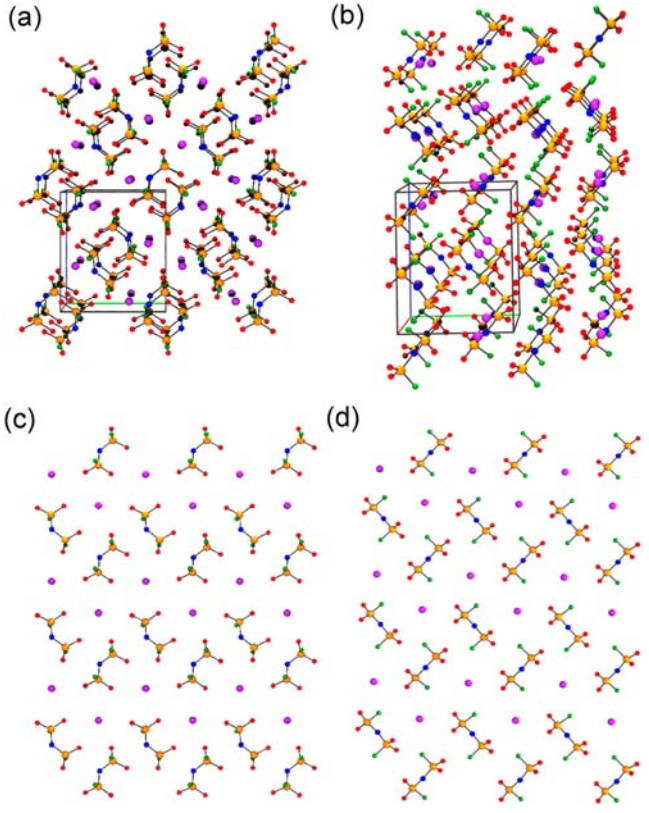

Figure 6. Packing diagrams of (a) $Cs[N(SO_2F)_2]$ (Form I) and (b) $Cs[N(SO_2F)_2]$ (Form II)[21] viewed along the *a*-axis. The ion configurations for (c) $Cs[N(SO_2F)_2]$ (Form I) and (d) $Cs[N(SO_2F)_2]$ (Form II) are also compared within their respective layers.[21].

O6, O8, and F4 cap the distorted trigonal prism], whereas K2 has an asymmetric nine-coordinate environment [K–O bond lengths = 2.6391(13)– 2.8824(13) Å, K–F bond lengths = 2.7716(11) and 3.3618(12) Å, and K–N bond lengths = 2.9443(14) and 3.0035(14) Å]. In $K[N(SO_2F)_2]$ (form II), K1 is in a nine-coordinate distorted tricapped trigonal-prismatic manner [K–O bond lengths = 2.655(6)–3.022(6) Å, K–F bond length = 2.966(5), and K–N bond length = 3.007(7) Å; O1, O4, and F4 cap the distorted trigonal prism] and K2 is in a 10-coordinate distorted bicapped square antiprism manner [K–O bond lengths = 2.660(6)–3.379(7) Å, K–F bond length = 2.922(5) Å, and K–N bond length = 3.188(7) Å; O3 and O6 cap the distorted square antiprism]. F atoms are involved in primary contacts in the cases of K2 in $K[N(SO_2F)_2]$ (form I) and K1 and K2 in $K[N(SO_2F)_2]$ (form II). The Cs cation in $Cs[N(SO_2F)_2]$ (form I) is 10-coordinate [one F, one N, six O, and two O/F disordered atoms; Cs–O bond lengths = 3.098(4)–3.502(4) Å, Cs–F bond lengths = 3.090(3)–3.320(3) Å, and Cs–N bond length = 3.328(4) Å], with a coordination environment best described as a distorted bicapped square antiprism (two O2 atoms cap the distorted square antiprism).

Raman Spectroscopy. The Raman spectra of $Na[N(SO_2F)_2]$, $K[N(SO_2F)_2]$, and $Cs[N(SO_2F)_2]$ at 298 K are shown in Figure 7. The frequencies, intensities, and assignments of the vibrational bands are provided in Tables S6–S8 in the Supporting Information. The Raman spectra of $Na[N(SO_2F)_2]$ (form II, cis), $K[N(SO_2F)_2]$ (form I, cis), $K[N(SO_2F)_2]$ (form II, cis), and $Cs[N(SO_2F)_2]$ (form II, trans) were assigned based

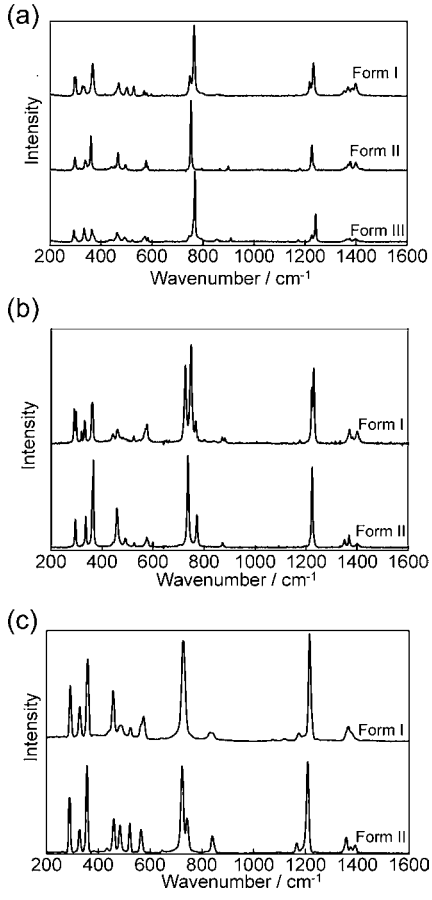

Figure 7. Raman spectra of (a) $Na[N(SO_2F)_2]$, (b) $K[N(SO_2F)_2]$, and (c) $Cs[N(SO_2F)_2]$ at 298 K.

dx.doi.org/10.1021/ic3010486 | Inorg. Chem. 2013, 52, 568–576

on the calculated *cis*- or *trans*-$N(SO_2F)_2^-$ structure because the crystallographic data revealed that these modifications have a single ordered anion.

Overall, the Raman spectra of the investigated $M[N(SO_2F)_2]$ salts closely resemble each other and are in good agreement with the calculated Raman frequencies of *cis*- and *trans*-$N(SO_2F)_2^-$ anions and the 21 fundamental modes that are expected. A previous report suggested that in the ionic liquid state ($[EMIm][N(SO_2F)_2]$, where EMIm = 1-ethyl-3-methylimidazolium) both the cis and trans conformers of the anion coexist, where the assignments were based on the calculated frequencies and intensities because the *cis*- and *trans*-$N(SO_2F)_2^-$ anions show slight differences in frequencies for several modes.[24] On the other hand, in the solid state, the Raman spectra are not sufficiently informative to distinguish the conformation of the anion because the structure of $N(SO_2F)_2^-$ does not exactly correlate with the calculated structure (see the torsion angles in Table 2). Thus, the frequency differences observed between the calculated cis and trans conformers are not sufficient in themselves to identify the conformer. For example, the intense peak assigned to the S−F stretching mode combined with the SO_2 and SNS scissoring modes is observed at 753 cm^{-1} for the cis conformer in $Na[N(SO_2F)_2]$ (form II) and at 727 and 746 cm^{-1} for the trans conformer in $Cs[N(SO_2F)_2]$ (form II), which agrees with the trend in the calculated values, where the calculated frequency for the cis conformer (709 cm^{-1}) is found to be larger than that of the trans conformer (697 cm^{-1}). On the other hand, the frequency of the $\delta_{op}(SO_2F) - \delta_{op}(SO_2F)$ mode for the cis conformer in $Na[N(SO_2F)_2]$ (form II) is observed at 278 cm^{-1}, which is lower than that observed for the $\rho_t(SO_2F) + \rho_t(SO_2F)$ mode of the trans conformer in $Cs[N(SO_2F)_2]$ (form II: 275 cm^{-1}), but an opposite trend is observed for the calculated frequencies. Another difficulty arises from factor-group splitting. If $N(SO_2F)_2^-$ is located at the general point under the space groups of *Pcab* (point group: D_{2h}) or $P2_1/n$ (point group: C_2) (Table S7 in the SI), the A mode for the cis conformer and the A and B modes for the trans conformer could split into several peaks in Raman spectra through factor-group splitting.[35] In conclusion, once the correspondence of the crystal structure with the Raman spectrum is established, Raman spectroscopy is useful for the identification of each phase in the $M[N(SO_2F)_2]$ series of salts.

Thermal Stabilities of Polymorphs. Schematic Gibbs free energy−temperature ($G-T$) diagrams for $Na[N(SO_2F)_2]$, $K[N(SO_2F)_2]$, and $Cs[N(SO_2F)_2]$ are shown in Figure 8. These diagrams are drawn based on the results of DSC, XRD, and Raman spectroscopy and additional observations as described below.

For $Na[N(SO_2F)_2]$, form II is more stable than form III at room temperature because the spontaneous transition from form III to form II was confirmed after long-term aging at room temperature. Form II is also considered to be more stable than form I unless the solid−solid transition from form II to form I has a large kinetic barrier. The resulting $G-T$ relationship for this trimorphic system is shown in Figure 8a.

In the case of $K[N(SO_2F)_2]$, form I is more stable than form II at room temperature because the phase transition from form II to form I spontaneously occurs after long-term aging or physical shock such as grinding in a mortar. A glass container entirely filled with $K[N(SO_2F)_2]$ in form II (obtained by the slow cooling of molten $K[N(SO_2F)_2]$) sometimes cracked when a phase transition to form I occurred because of the difference in volume (formula unit volume at 298 K: 154.3 $Å^3$ for form I at room temperature and 152.9 $Å^3$ for form II). The resulting $G-T$ diagram is typical of a monotropic system (Figure 8b).

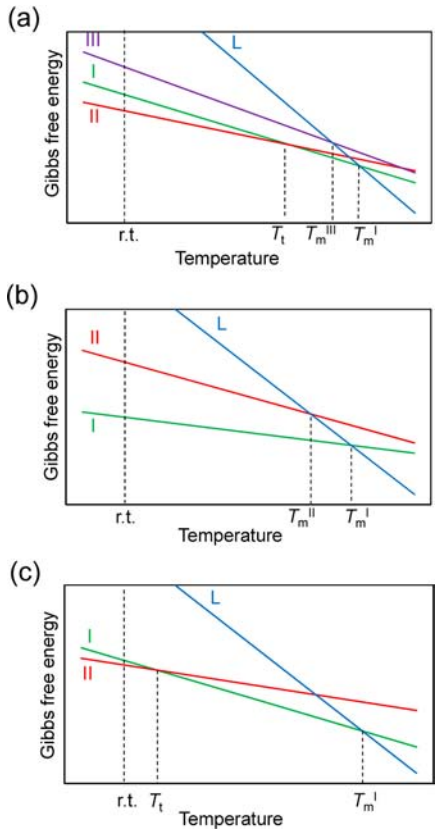

Figure 8. Schematic Gibbs free energy−temperature ($G-T$) diagrams for $Na[N(SO_2F)_2]$, $K[N(SO_2F)_2]$, and $Cs[N(SO_2F)_2]$. The abbreviations r.t., T_t, and T_m denote room temperature, solid−solid transition temperature, and melting temperature, respectively.

The first-order solid−solid transition from form II to form I at 330 K suggests that the two forms of $Cs[N(SO_2F)_2]$ are enantiotropically related. Although the transition from one form to the other form did not occur at room temperature, the stable form at room temperature is considered to be form II, assuming that the solid−solid transition from form II to form I observed at 330 K does not have a large kinetic barrier. The resulting $G-T$ diagram is shown in Figure 8c.

■ CONCLUSIONS

In conclusion, the polymorphism of $M[N(SO_2F)_2]$ (M = Na, K, and Cs) has been investigated by means of DSC, single-crystal and powder XRD, and Raman spectroscopy. The polymorphism (three forms for $Na[N(SO_2F)_2]$, two forms for $K[N(SO_2F)_2]$, and two forms for $Cs[N(SO_2F)_2]$) arises from the cis−trans conformational difference of $N(SO_2F)_2^-$ as well as from differences in the crystal packing. Disorder of $N(SO_2F)_2^-$ is observed for form I of $Na[N(SO_2F)_2]$ at 298 K (cis−trans disorder) and form I of $Cs[N(SO_2F)_2]$ at 113 K (oxygen/fluorine disorder based on an eclipsed conformation). The $G-T$ diagrams of the three salts are drawn based on these analyses. In the case of $Na[N(SO_2F)_2]$, form III is monotropically related to forms I and II, and form II with *cis*-$N(SO_2F)_2^-$ is the most stable of them at room temperature. The behavior of $K[N(SO_2F)_2]$ and $Cs[N(SO_2F)_2]$ suggests that they belong to monotropic and enantiotropic systems, respectively. The stable forms are form I

dx.doi.org/10.1021/ic3010486 | *Inorg. Chem.* 2013, 52, 568−576

with *cis*-$N(SO_2F)_2^-$ for $K[N(SO_2F)_2]$ and form II with *trans*-$N(SO_2F)_2^-$ for $Cs[N(SO_2F)_2]$.

EXPERIMENTAL SECTION

Apparatus and Materials. Volatile materials were handled in a vacuum line constructed using stainless steel, Pyrex glass, and tetrafluoroethylene−perfluoroalkyl vinyl ether copolymer. Nonvolatile materials were handled under a dry argon atmosphere in a glovebox. The Na and K salts, $Na[N(SO_2F)_2]$ (Mitsubishi Materials Electronic Chemicals Co., Ltd.; purity >99.0%) and $K[N(SO_2F)_2]$ (Mitsubishi Materials Electronic Chemicals Co., Ltd.; purity >99.0%), respectively, were dried at 353 K for 24 h prior to use. The Cs salt, $Cs[N(SO_2F)_2]$, was prepared and purified according to the literature method.[31] Anhydrous ethanol (Wako Chemicals; water content <50 ppm) and anhydrous 2-propanol (Wako Chemicals; water content <50 ppm) were used as received. Anhydrous hydrogen fluoride (HF; Daikin Industries Co., Ltd.; purity >99%) was dried over K_2NiF_6 (Ozark-Mahoning Co.) for several days prior to use (for treatment of anhydrous HF, see previous work[36,37]).

Spectroscopic and Thermal Analyses. Raman spectra were recorded (Horiba Jobin Yvon, LabRAM300) at room temperature using the 633-nm line of a He−Ne laser as the excitation line and 1 cm^{-1} resolution. The samples for Raman spectroscopy were loaded in an aluminum pan, which was sealed in an airtight unit with a glass window. DSC (DSC-60, Shimadzu) was performed under a dry argon gas flow. The samples for DSC measurement were loaded into aluminum airtight cells under dry argon. A scan rate of 10 K min^{-1} was used.

XRD Analyses. *a. Powder XRD.* The sample was well-ground and transferred into a quartz capillary (0.5 mm o.d., dried under vacuum at 773 K prior to use) under a dry argon atmosphere. The capillary was temporarily plugged with vacuum grease and sealed using an oxygen torch. The sample was centered on an R-axis Rapid II X-ray diffractometer (Rigaku Corp.) equipped with an imaging-plate area detector (using the program *RAPID XRD 2.3.3*[38]) and exposed to graphite-monochromated Mo Kα irradiation (0.71073 Å, 50 kV, and 40 mA). The φ angle was rotated at a rate of 1° s^{-1}, and the ω and χ angles were fixed at 20° and 0°, respectively, during data collection (720 s). Another X-ray diffractometer, Ultima IV (Rigaku Corp.), equipped with a scintillation counter detector and graphite-monochromated Cu Kα irradiation (1.5418 Å, 40 kV, and 40 mA) was also used. The sample for Ultima IV was spread on a glass sample holder and covered with parafilm to avoid contact with the air. Simulation of powder XRD patterns based on single-crystal X-ray structures was performed using the program *Powder Cell*.[39]

b. Single-Crystal XRD. Single-crystal XRD was performed using the R-axis Rapid II (Rigaku Corp.) diffractometer controlled by the program *RAPID AUTO 2.40*[40]). Crystals of $Na[N(SO_2F)_2]$ (form I), $K[N(SO_2F)_2]$ (form II), and $Cs[N(SO_2F)_2]$ (form I) were grown by repeated slow solidification from the molten salts in a quartz capillary on the goniometer. Single crystals of $Na[N(SO_2F)_2]$ (form II) were grown by the slowly removal of the solvent from a saturated anhydrous HF solution at room temperature. Single crystals of $K[N(SO_2F)_2]$ (form I) were grown by the slow cooling of a saturated 2-propanol solution from 323 K to room temperature. Suitable crystals were mounted in quartz capillaries under dry argon and sealed in the same manner as that for the powder sample. Data collection was performed at 113 and 298 K and consisted of 12 ω scans (130−190° and 5° $frame^{-1}$) at fixed φ (0°) and χ (45°) angles and 32 ω scans (0−160° and 5° $frame^{-1}$) at fixed φ (180°) and χ (45°) angles. The exposure times were 100 s deg^{-1} (113 and 298 K) for $Na[N(SO_2F)_2]$ (form I), 200 s deg^{-1} (113 K) and 300 s deg^{-1} (298 K) for $Na[N(SO_2F)_2]$ (form II), 100 s deg^{-1} (113 K) and 200 s deg^{-1} (298 K) for $K[N(SO_2F)_2]$ (form I), and 150 s deg^{-1} (113 K) and 400 s deg^{-1} (298 K) for $K[N(SO_2F)_2]$ (form II), and 150 s deg^{-1} (113 and 298 K) for $Cs[N(SO_2F)_2]$ (form I). Integration, scaling, and absorption corrections were performed using *RAPID AUTO 2.40*. The structure was solved using *SIR-92*[41] and refined by *SHELXL-97*[42] linked to *Win-GX*.[43] Anisotropic displacement factors were introduced for all atoms. One of the two $N(SO_2F)_2^-$ anions was solved based on a cis−trans disorder model. The S−F (S2−F2A and S2−F2B) and S−O (S2−O3A and S2−O3B) bond lengths were separately constrained by the DFIX instruction. The $N(SO_2F)_2^-$ anion in $Cs[N(SO_2F)_2]$ (form I) at 113 and 298 K was solved based on the oxygen/fluorine disorder model. The atomic coordinates of the O and F atoms ([O3A, F2B] and [O3B, F2A]) were restrained by the EXYZ instruction, and the atomic displacement factors of the O and F atoms ([O3A, F2B] and [O3B, F2A]) were restrained by the EADP instruction.

Calculations. The energy-minimized gas-phase structures, volumes, and vibrational frequencies and intensities were calculated at the PBE1PBE and MP2 levels of theory using cc-pVTZ and aug-cc-pVTZ basis sets. Quantum-chemical calculations were carried out using the program *Gaussian 03*.[44]

ASSOCIATED CONTENT

Supporting Information

X-ray crystallographic data in CIF format, single-crystal and powder XRD data, effects of vessels on the crystallization of $K[N(SO_2F)_2]$, calculated geometrical parameters, and experimental and calculated vibrational frequencies and intensities as well as correlation diagrams for factor-group analysis. This material is available free of charge via the Internet at http://pubs.acs.org.

AUTHOR INFORMATION

Corresponding Author

*E-mail: k-matsumoto@energy.kyoto-u.ac.jp.

Notes

The authors declare no competing financial interest.

ACKNOWLEDGMENTS

This study was partly supported by Grants-in-Aid for Scientific Research A (Grant 20246140) from JSPS and by the Advanced Low Carbon Technology Research and Development Program (ALCA) of JST.

REFERENCES

(1) Vij, A.; Kirchmeier, R. L.; Shreeve, J. M.; Verma, R. D. *Coord. Chem. Rev.* **1997**, *158*, 413−432.
(2) Best, A. S.; Bhatt, A. I.; Hollenkamp, A. F. *J. Electrochem. Soc.* **2010**, *157*, A903−A911.
(3) Macfarlane, D. R.; Forsyth, M.; Howlett, P. C.; Pringle, J. M.; Sun, J.; Annat, G.; Neil, W.; Izgorodina, E. I. *Acc. Chem. Res.* **2007**, *40*, 1165−1173.
(4) Ohno, H. *Electrochemical Aspects of Ionic Liquids*, 2nd ed.; John Wiley & Sons Inc.: Hoboken, NJ, 2011.
(5) Armand, M.; Endres, F.; MacFarlane, D. R.; Ohno, H.; Scrosati, B. *Nat. Mater.* **2009**, *8*, 621−629.
(6) Ishikawa, M.; Sugimoto, T.; Kikuta, M.; Ishiko, E.; Kono, M. *J. Power Sources* **2006**, *162*, 658−662.
(7) Matsumoto, H.; Sakaebe, H.; Tatsumi, K.; Kikuta, M.; Ishiko, E.; Kono, M. *J. Power Sources* **2006**, *160*, 1308−1313.
(8) Guerfi, A.; Duchesne, S.; Kobayashi, Y.; Vijh, A.; Zaghib, K. *J. Power Sources* **2008**, *175*, 866−873.
(9) Han, H. B.; Nie, J.; Liu, K.; Li, W. K.; Feng, W. F.; Armand, M.; Matsumoto, H.; Zhou, Z. B. *Electrochim. Acta* **2010**, *55*, 1221−1226.
(10) Zaghib, K.; Charest, P.; Guerfi, A.; Shim, J.; Perrier, M.; Striebel, K. *J. Power Sources* **2004**, *134*, 124−129.
(11) Abouimrane, A.; Ding, J.; Davidson, I. J. *J. Power Sources* **2009**, *189*, 693−696.
(12) Li, L. F.; Zhou, S. S.; Han, H. B.; Li, H.; Nie, J.; Armand, M.; Zhou, Z. B.; Huang, X. J. *J. Electrochem. Soc.* **2011**, *158*, A74−A82.
(13) Han, H. B.; Zhou, S. S.; Zhang, D. J.; Feng, S. W.; Li, L. F.; Liu, K.; Feng, W. F.; Nie, J.; Li, H.; Huang, X. J.; Armand, M.; Zhou, Z. B. *J. Power Sources* **2011**, *196*, 3623−3632.
(14) Dahbi, M.; Ghamouss, F.; Tran-Van, F.; Lemordant, D.; Anouti, M. *J. Power Sources* **2011**, *196*, 9743−9750.

(15) Sawyer, J. F.; Schrobilgen, G. J.; Sutherland, S. J. *J. Chem. Soc., Chem. Commun.* **1982**, 210−211.
(16) Sawyer, J. F.; Schrobilgen, G. J.; Sutherland, S. J. *Inorg. Chem.* **1982**, *21*, 4064−4072.
(17) Desmarteau, D. D.; Leblond, R. D.; Hossain, S. F.; Nothe, D. *J. Am. Chem. Soc.* **1981**, *103*, 7734−7739.
(18) Leblond, R. D.; Desmarteau, D. D. *J. Chem. Soc., Chem. Commun.* **1974**, 555−556.
(19) Zak, Z.; Ruzicka, A.; Michot, C. *Z. Kristallogr.* **1998**, *213*, 217−222.
(20) Beran, M.; Prihoda, J.; Zak, Z.; Cernik, M. *Polyhedron* **2006**, *25*, 1292−1298.
(21) Hiemisch, O.; Henschel, D.; Blaschette, A.; Jones, P. G. *Z. Anorg. Allg. Chem.* **1997**, *623*, 324−332.
(22) Farrugia, L. J.; Holfter, H.; Klapotke, T. M. *J. Fluorine Chem.* **1996**, *78*, 51−53.
(23) Faggiani, R.; Kennepohl, D. K.; Lock, C. J. L.; Schrobilgen, G. J. *Inorg. Chem.* **1986**, *25*, 563−571.
(24) Fujii, K.; Fujimori, T.; Takamuku, T.; Kanzaki, R.; Umebayashi, Y.; Ishiguro, S. I. *J. Phys. Chem. B* **2006**, *110*, 8179−8183.
(25) Lopes, J. N. C.; Shimizu, K.; Padua, A. A. H.; Umebayashi, Y.; Fukuda, S.; Fujii, K.; Ishiguro, S. I. *J. Phys. Chem. B* **2008**, *112*, 9449−9455.
(26) Tsuzuki, S.; Hayamizu, K.; Seki, S. *J. Phys. Chem. B* **2010**, *114*, 16329−16336.
(27) Begley, M. J.; Sowerby, D. B.; Verma, R. D.; Vig, A. *J. Organomet. Chem.* **1994**, *481*, 243−246.
(28) Isenberg, W.; Noltemeyer, M.; Sheldrick, G. M. *Acta Crystallogr., Sect. B* **1982**, *38*, 2887−2889.
(29) Kubota, K.; Nohira, T.; Hagiwara, R. *J. Chem. Eng. Data* **2010**, *55*, 3142−3146.
(30) Kubota, K.; Nohira, T.; Goto, T.; Hagiwara, R. *Electrochem. Commun.* **2008**, *10*, 1886−1888.
(31) Kubota, K.; Tamaki, K.; Nohira, T.; Takuya, G.; Hagiwara, R. *Electrochim. Acta* **2012**, *66*, 320−324.
(32) Fukunaga, A.; Nohira, T.; Kozawa, Y.; Hagiwara, R.; Sakai, S.; Nitta, K.; Inazawa, S. *J. Power Sources* **2012**, *209*, 52−56.
(33) In this study, both structures at 113 and 298 K are treated as form I for simplicity, although these two structures can be regarded as different phases in terms of disordering.
(34) Lork, E.; Mews, R.; Viets, D.; Watson, P. G.; Borrmann, T.; Vij, A.; Boatz, J. A.; Christe, K. O. *Inorg. Chem.* **2001**, *40*, 1303−1311.
(35) Carter, R. L. *J. Chem. Educ.* **1971**, *48*, 297−303.
(36) Matsumoto, K.; Hagiwara, R. *J. Fluorine Chem.* **2011**, *131*, 805−808.
(37) Peters, D.; Miethchen, R. *J. Fluorine Chem.* **1996**, *79*, 161−165.
(38) *RAPID XRD 2.3.3*; Rigaku Corp.: Tokyo, 1999−2004.
(39) Krauss, W.; Nolze, G. *Powder Cell 2.3 for Windows*; Federal Institute for Materials Reserach and Testing: Berlin, 1999.
(40) *RAPID AUTO 2.40*; Rigaku Corp.: Tokyo, 2006.
(41) Altomare, A.; Cascarano, G.; Giacovazzo, C.; Guagliardi, A. *J. Appl. Crystallogr.* **1993**, *26*, 343−350.
(42) Sheldrick, G. M. *Acta Crystallogr., Sect. A* **2008**, *64*, 112−122.
(43) Farrugia, L. J. *J. Appl. Crystallogr.* **1999**, *32*, 837−838.
(44) Frisch, M. J.; Trucks, G. W.; Schlegel, H. B.; Scuseria, G. E.; Robb, M. A.; Cheeseman, J. R.; Montgomery, J. A., Jr.; Vreven, T.; Kudin, K. N.; Burant, J. C.; Millam, J. M.; Iyengar, S. S.; Tomasi, J.; Barone, V.; Mennucci, B.; Cossi, M.; Scalmani, G.; Rega, N.; Petersson, G. A.; Nakatsuji, H.; Hada, M.; Ehara, M.; Toyota, K.; Fukuda, R.; Hasegawa, J.; Ishida, M.; Nakajima, T.; Honda, Y.; Kitao, O.; Nakai, H.; Klene, M.; Li, X.; Knox, J. E.; Hratchian, H. P.; Cross, J. B.; Bakken, V.; Adamo, C.; Jaramillo, J.; Gomperts, R.; Stratmann, R. E.; Yazyev, O.; Austin, A. J.; Cammi, R.; Pomelli, C.; Ochterski, J. W.; Ayala, P. Y.; Morokuma, K.; Voth, G. A.; Salvador, P.; Dannenberg, J. J.; Zakrzewski, V. G.; Dapprich, S.; Daniels, A. D.; Strain, M. C.; Farkas, O.; Malick, D. K.; Rabuck, A. D.; Raghavachari, K.; Foresman, J. B.; Ortiz, J. V.; Cui, Q.; Baboul, A. G.; Clifford, S.; Cioslowski, J.; Stefanov, B. B.; Liu, G.; Liashenko, A.; Piskorz, P.; Komaromi, I.; Martin, R. L.; Fox, D. J.; Keith, T.; Al-Laham, M. A.; Peng, C. Y.; Nanayakkara, A.; Challacombe, M.; Gill, P. M. W.; Johnson, B.; Chen, W.; Wong, M. W.; Gonzalez, C.; Pople, J. A. *Gaussian 03*; Gaussian Inc.: Wallingford, CT, 2004.